Journal of
Materials Chemistry B

Materials for biology and medicine

Accepted Manuscript

This article can be cited before page numbers have been issued, to do this please use: S. Vasudevan, P. Srinivasan , J. B. B. Rayappan and A. P. Solomon, *J. Mater. Chem. B*, 2020, DOI: 10.1039/C9TB02243K.

ROYAL SOCIETY OF CHEMISTRY

rsc.li/materials-b

View Article Online
DOI: 10.1039/C9TB02243K

Photoluminescence Biosensor for the Detection of *N*-Acyl Homoserine Lactone using Cysteamine functionalized ZnO Nanoparticles for the Early Diagnosis of Urinary Tract Infection

Sahana Vasudevan[a#], Parthasarathy Srinivasan[b#], John Bosco Balaguru Rayappan[b*#] and Adline Princy Solomon[a*#]

[a] *Quorum Sensing Laboratory, School of Chemical and Biotechnology, SASTRA Deemed to be University, Thanjavur, 613401, Tamilnadu, India.*

[b] *Nanosensors Laboratory, School of Electrical & Electronics Engineering, Centre for Nanotechnology & Advanced Biomaterials (CeNTAB), SASTRA Deemed University, Thanjavur 613401, Tamilnadu, India.*

* Corresponding author; # equal contribution

Graphical Abstract:

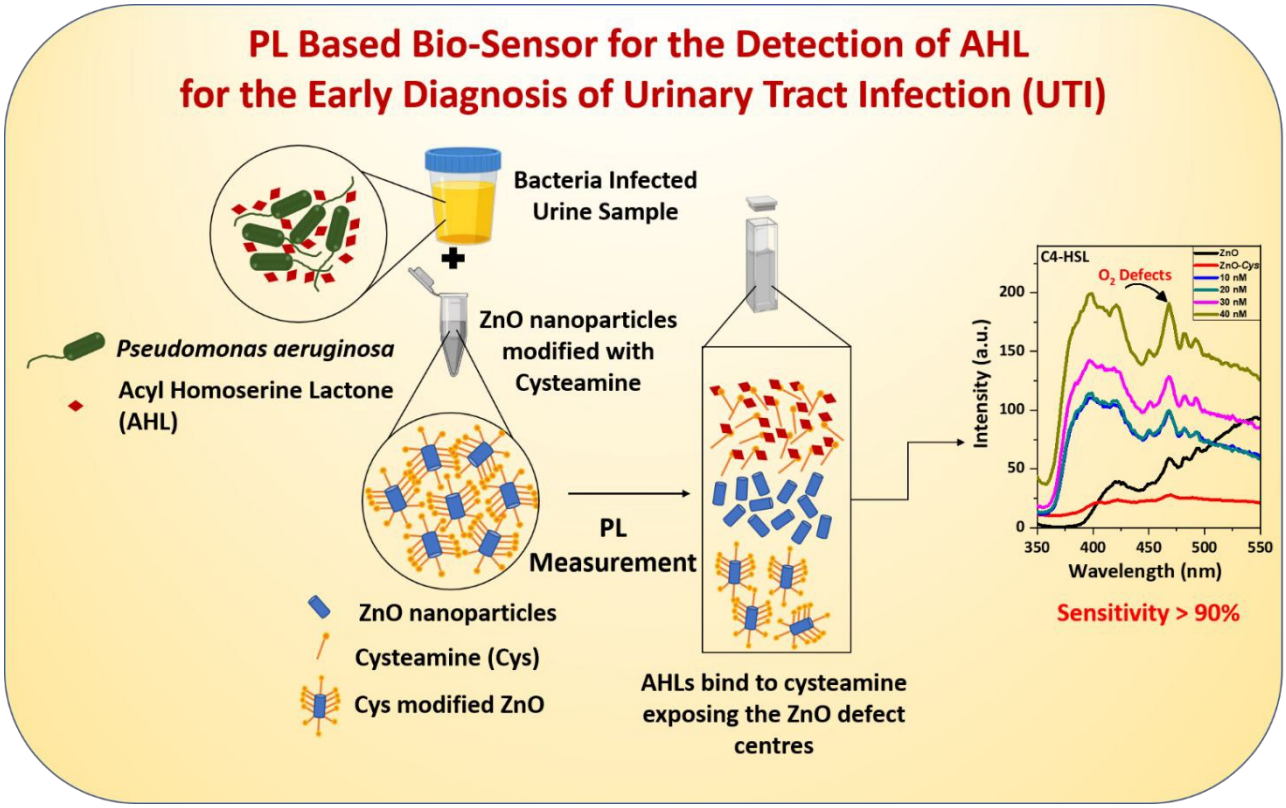

We report the PL bio-sensor using Cysteamine functionalized ZnO nanoparticles for the detection of quorum sensing signals (*N*-Acyl Homoserine Lactones).

View Article Online
DOI: 10.1039/C9TB02243K

Abstract:

Urinary Tract Infection (UTI) is a recurrent infection that requires timely diagnosis and appropriate treatment. The conventional urinalysis methods are laborious and time-consuming, which lacks sensitivity and specificity. In this context, photoluminescence (PL)-based biosensor has gained more attention due to its fast response time, enhanced sensitivity and specificity. Towards this, PL based biosensor was developed using microwave-assisted ZnO nanoparticles functionalized with cysteamine (ZnO-*Cys*) to detect quorum sensing signalling molecules of Gram-negative bacteria, *N*-Acyl-Homoserine Lactones (AHLs). These AHLs are involved in bacterial communication and are responsible for activating virulence and pathogenicity. Biosensing measurements based on PL intensity variations corresponding to the O_2 acceptor defect level of ZnO with reference to the ZnO-*Cys* was considered. The maximum sensitivity of 97% was achieved towards the detection of AHL. The linear detection range of the developed biosensor was observed to be 10-120 nM in Artificial Urine Media (AUM). The effect of pH on the sensitivity in the AUM was also investigated and reported. The developed sensor was validated for the AHLs produced by *Pseudomonas aeruginosa* (MCC3101) in real-time analysis, which further confirmed the overall specificity and sensitivity.

Keywords: UTI, ZnO nanoparticles, Cysteamine, Quorum Sensing, Acyl Homoserine Lactone, Photoluminescence.

View Article Online
DOI: 10.1039/C9TB02243K

1. Introduction

Urinary Tract Infections (UTIs) are most common among people with millions of cases have been reported every year [1]. UTIs are considered as the second common cause of infectious disease with the high recurrence rate affecting patients in all demographics [2]. Even with such high incidence, the diagnosis is only based on symptomatology and urine culture. Urine dipstick analysis is the conventional technique used for detecting nitrites and leukocyte esterase. However, the lack of sensitivity and specificity limits its usage in real-time analysis[3]. Also, the clinical diagnosis requires urine culture and gram stain, which are laborious and time-consuming. In this context, clinical molecular platforms like Matrix-Assisted Laser Desorption Ionization (MALDI-TOF), Fluorescence *in-situ* Hybridization (FISH) and Polymerase Chain Reaction (PCR) have been considered as a viable alternative to overcome major drawbacks of conventional clinical techniques. Nevertheless, these techniques are again time-consuming owing to the sample processing for sample processing and isolation of bacteria from the urine before analysis [4]. Hence, it is imperative to design and develop highly accurate, efficient and rapid biosensor with minimum or no sample processing for the early diagnosis of UTI.

Selecting a suitable biomarker (bio-analyte) for the detection of UTI is a prerequisite, as it decides the overall sensing signatures. UTIs are majorly caused by *Escherichia coli*, *Klebsiella pneumoniae*, *Proteus mirabilis,* and *Enterobacter* species. *E. coli,* which are responsible for 85–90% of cases accounting for cystitis and pyelonephritis, making it the most common urinary pathogen [2]. It is evidenced that polymicrobial interaction leads to increased virulence in UTIs. This interaction is facilitated by quorum sensing,

View Article Online
DOI: 10.1039/C9TB02243K

where the bacteria releases specific signal molecules, which is identified by self (intra-species communication) and other bacteria (inter-species communication). In the case of Gram-negative bacteria, AHL is the signaling molecule that is produced by the majority of the uropathogens during the infection process[5]. Therefore, AHL can be considered as an appropriate analyte for the biosensing of UTI.

AHL molecule facilitates inter-species communication between *P. aeruginosa* and *E. coli*. *P*. *aeruginosa,* a common UTI pathogen, produces two distinct types of AHL: *N*-(3-oxododecanoyl) - homoserine lactone (OdDHL or 3OC12-HSL) and *N*-Butanoyl homoserine lactone (BHL or C4- HSL) [6]. *E. coli*, on the other hand, does not synthesize AHL but has SdiA, a receptor that can recognize exogenous AHLs and regulate virulence gene expression [7]. This sets up a unique cross-talk between the two species through the AHL molecule. In addition to the above AHLs, *E. coli* can sense and detect AHL molecules synthesized by other uropathogens. This includes C6-HSL and 3-oxo forms of AHL, which facilitates the interspecies communication[8]. The presence and the role of these signal molecules in the host damage are well documented [9]. Hence, through this study, we seek to rely on this communication signal, AHL, for the detection and diagnosis of UTI. The correlation between the levels of AHL produced to a load of infection and virulence forms the crux of the sensing. Sensing of the AHL, employing a nano-optical detection technique, may serve as a biomarker to diagnose UTI due to its active participation in the quorum sensing mechanism and virulence. In this context, metal oxide semiconductor materials are immediate choices for the development of optoelectronic devices due to electroluminescence, strong photoluminescence (PL), or nonlinear optical behavior[10]. PL based biosensors are advantageous in terms of achieving higher sensitivity with lower interference.

View Article Online
DOI: 10.1039/C9TB02243K

ZnO is an n-type metal-oxide semiconducting material, which has been in the center of attraction over the years in many applications, especially in optical-based sensing devices[11–13]. The characteristic emissions band of ZnO is in the ultraviolet (UV) region and corresponds to the near band – edge emission [14] and visible regions. A recent review on ZnO nanoparticles highlights the advantages of using them as optical biosensors. Various bio-analytes such as dopamine, glucose, protein, salmonella antigen, and avidin-horseradish peroxidase have been sensed by exploiting the PL property of ZnO nanoparticles[15].

To promote the effective interaction between the ZnO nanoparticles and AHL, a well-known non-toxic linker molecule, cysteamine has been considered. Cysteamine is an FDA approved drug used in the treatment of neurological disorders, cystinuria and cystinosis. This simple aminothiol is involved in critical physiological processes, including the development of an embryo, synthesis of protein and also has radioprotective effect[16]. The presence of the reactive groups amine and thiol makes it an obvious choice as a linker molecule[17–20]. Furthermore, Cysteamine has been reported for active functionalization with ZnS and CdS quantum dots for the detection of aflatoxin using PL based bio-sensing principle [17,18]. In this background, the present investigation dealt with the development of PL based AHL biosensor using cysteamine functionalized ZnO nanoparticles. The sensitivity of the system is based on the PL intensity variations, which is dependent on AHL concentration. The versatility of the sensor system is established by the interaction studies with short (C4 HSL), medium (C6 HSL), and long-chain AHL (3O C12 HSL) molecules. The sensitivity and specificity were evaluated in the presence of AUM, which mimics the composition of the urine. It was established that ZnO-*Cys* was sensitive and specific to AHL detection even in the presence of interferences. Thus, the ZnO-

Cys biosensor system can be used for the rapid detection of the AHL molecule and thereby the diseased condition.

2. Materials and methods

2.1 Microwave synthesis of ZnO nanoparticles

0.1 M of zinc chloride $ZnCl_2$ (Sigma Aldrich, USA) was dissolved in 100 mL of deionized water and kept in the commercial microwave oven at the constant microwave power of 450 W for 30 min. The precipitate obtained was centrifuged successively and cleaned several times with ethanol and water, respectively. The prepared nanoparticles were annealed at 343 K for 3 h and calcined at 523 K for 5 h to obtain ZnO nanoparticles.

2.2 Functionalization of Cysteamine with ZnO nanoparticles

The prepared ZnO nanoparticles were dispersed in ethanol media. The linker molecule, cysteamine, was added to the ZnO nanoparticles solution in three different ratios (1:0.5, 1:1 and 0.5:1) and stirred for 12 h to yield homogeneous organic ligand immobilized solution.

2.3 Characterization

Morphology of the prepared nanoparticles was observed using Field Emission Scanning Electron Microscope (JSM-6701F, JEOL, Japan). Structural characteristics of the prepared nanoparticles were studied using an X-ray diffractometer (XRD, Bruker, Model D8 Focus, Germany). Surface defects of the prepared nanoparticles were investigated using the PL spectrophotometer (FP 8200, JASCO, USA). Zeta potential and

View Article Online
DOI: 10.1039/C9TB02243K

particle size measurements were carried out using the Zeta sizer system (Nano-ZS, Malvern Instruments, UK). Functional group analysis was studied using Fourier transform infrared spectrometer (Bruker, Alpha-T, Germany).

2.4 Preparation of Bio-analyte and Artificial Urine Media

N-Acyl Homoserine Lactones (AHLs): C4-HSL (N-Butyryl-DL-homoserine lactone, ≥96.0%), C6-HSL (*N*-hexanoyl-L-homoserine lactone) and 3-Oxo-C_{12}-HSL (*N*-(3-oxododecanoyl)- homoserine lactone) were obtained from Sigma Aldrich, USA and dissolved in DMSO (Sigma Aldrich). The resultant solution was taken as a bio-analyte for sensing studies. AUM was prepared according to the previous report [21]. The components of the AUM are highlighted in Table S1.

2.5 Biosensing measurements

Biosensing measurements were carried out using a PL spectrophotometer (FP 8200, JASCO, USA). Emission and excitation bandwidth of 5 nm were maintained throughout the experiment. The excitation wavelength of ZnO nanoparticles was maintained at 320 nm for observing the emission spectra in the range of 350-550 nm. The response time of the detector was kept as 1 s with a recording speed of 500 nm/min at room temperature. PL spectra of the ZnO nanoparticles, ZnO-*Cys,* and ZnO-*Cys* in the presence of different AHL (C4, C6 and 3-oxo-C_{12}) were recorded to observe the sensitivity. The sensitivity of the biosensor was calculated using the relation expressed in Eq. (1) as,

$$S = \frac{S_A - S_B}{S_A} X\ 100\ \% \quad (1)$$

where S denotes sensitivity, S_A is the peak intensity of ZnO-*Cys* in the presence of AHL, and S_B denotes the peak intensity of ZnO-*Cys* in the absence of AHL. The biosensing ability was tested by varying the AHL concentration from 10 to 40 nM and the relationship between the sensitivity and AHL concentration was investigated. The same protocol was followed in the presence of AUM to validate the specificity and sensitivity against potential interferents. Different HSL molecules at concentrations ranging from 10 nM to 1 µM were dissolved in AUM and analyzed.

2.6 Real-time analysis of ZnO- *Cys* with *P. aeruginosa*

ZnO- *Cys* was tested to identify the indigenously produced HSL of the human kidney stone isolated *Pseudomonas aeruginosa* (MCC3101). *P. aeruginosa* (OD_{595} = 0.05) was inoculated in AUM and incubated at 37°C. PL spectra were recorded at the interval of 30 mins to understand the time-dependent HSL detection by the ZnO-*Cys* system.

3.Results and discussion

3.1 Surface characterization of ZnO and ZnO-*Cys* nanoparticles

X-ray diffraction pattern of the prepared ZnO nanoparticles is shown in Fig. 1(a(i)). The observed pattern is in good agreement with the JCPDS card data [75-0576], which revealed the formation of polycrystalline natured, a primitive hexagonal lattice of ZnO with lattice parameters of a= 3.242 Å and c= 5.194 Å respectively. Preferential plane orientation was observed to be along (101) plane. XPS survey spectra of the prepared

View Article Online
DOI: 10.1039/C9TB02243K

nanoparticles are shown in Fig. 1(a (ii)) and the presence of Zn and O elements were identified. The peak at 531.1 eV correspond to O 1s spectra is attributed to the oxygen deficiencies in Zn-O interaction [22] (Fig. 1(a(iii))). The Zn 2p spectra observed at the binding energies of 1021 and 1044.1 eV represent Zn $2p_{3/2}$ and Zn $2p_{1/2,}$ respectively (Fig. 1(a)(iv)). The binding energy difference between these two states was found to be 23.1 eV, which confirmed the presence of Zn^{2+} oxidation states[13,23,24].

Surface morphologies of the ZnO and ZnO-*Cys* system are shown in Fig. 1 (b). Morphology of ZnO nanoparticles revealed the formation of non-homogeneously distributed, aggregated, and clustered nanorods. Grains were observed to be irregularly arranged due to the influence of thermal energy gradients developed during the microwave irradiation. In general, Cl^- ions from the precursor solution mediates the growth in the formation of distinct nanorods [25]. Also, the rate of Zn^{2+} dissociation from the $ZnCl_2$ precursor influences the shape factor. In the present case, the crumbled nanorods like morphology revealed the pronounced effect of thermal energy gradients in which it hinders the effect of Cl^- ions for further growth of nanorods [25].

In general, the functionalization provides a significant change in the morphology and size of the nanoparticles[26,27]. In the present case, there were no drastic changes in the shapes of the particles were observed (Fig. 1 (b) (ii)). Also, the existence of some larger sized particles was observed from the morphology with a minimal aggregation as compared to the ZnO nanoparticles. The particle size and zeta potential measurements of ZnO and Cys functionalized ZnO were repeated three times (n=3) to estimate the mean and standard deviations. The mean sizes of the ZnO and Cys functionalized ZnO nanoparticles were found to be 794.1±2.76 nm and 586.7±1.93 nm, respectively (Fig. S1). The decrease in the particle size of cysteamine functionalized ZnO may be attributed to the reduced agglomeration caused

by the dispersive effect[26,27]. The mean zeta potentials of ZnO and Cys functionalized ZnO nanoparticles were observed to be -45.4±3.39 and -14.41±1.25 mV, respectively. To understand further, the particle sizes of ZnO before and after functionalization was estimated from SEM images using Image J software. The average particle size distribution of ZnO before and after functionalization were found to be 758.5 and 592.7 nm respectively (Fig. S2 (a-b)). Though there is an existence of some larger sized nanoparticles after functionalization, the majority of the particles were distributed in the size range of 550-600 nm as depicted from the Fig. S2 (b). This trend is in good agreement with the particle sizes measured from zeta sizer. Also, the polydispersity index (PDI) values of ZnO and ZnO-Cys system were found to be 0.343 and 0.352 respectively. An increase in the PDI value of ZnO-Cys system supports the size effect with a minimal aggregation.

3.2 PL based Biosensing Measurements

3.2.1 Effect of ZnO-*Cys* ratio on AHL Sensitivity

To investigate the optimal concentration of cysteamine functionalization in ZnO, three different ratios of ZnO: *Cys* were considered as 1:0.5 and 0.5:1 along with a 1: 1 ratio, as shown in Fig. 2(a-d). The PL signatures of these three samples were examined towards varying concentrations (10 nM to 40 nM) of C4, C6, and 3-Oxo-C12 HSL, respectively.

When the amount of ZnO exceeds the concentration of the functionalizing material (Cysteamine) (i.e., the ratio of 1:0.5), the sensitivity was decreased (Fig. 2(a-d)). This is because the exposed defect centres of ZnO are least covered with the cysteamine molecules for AHL interaction. In other words, the incomplete capping effect of cysteamine with ZnO made the system least sensitive[17]. Similarly, in the case of 0.5:1 ratio of ZnO: Cysteamine, the sensitivity

View Article Online
DOI: 10.1039/C9TB02243K

was very less due to the excessive coverage of cysteamine with the ZnO surface. But for the 1:1 case, the defect centres are well exposed with the cysteamine molecules and facilitates the profound active sites for the AHL to interact in-turn showed maximum sensitivity. Hence, we have fixed this ratio as optimal for further bio-sensing measurements.

3.2.2 PL based AHL detection using ZnO-*Cys*

The defect profile of the prepared ZnO nanoparticles was observed using PL spectra at an excitation wavelength of 320 nm, as shown in Fig. 3. The intrinsic defect states were identified at 398, 421,450, 468, 482 and 492 nm [28,29]. The peak at 398 nm is attributed to the shifting of electrons from the conduction band of ZnO to single ionized oxygen vacancy [13,30,31]. This single ionized oxygen vacancy state induces the acceptor defect level just above the valance band of ZnO[13,14]. The peak at 421 nm corresponds to Zn^{2+} interstitial defect [13,32]. The shoulder peak observed at 450 nm corresponds to the doubly ionized Zn vacancy centers [33]. The sharp peak at 468 nm is attributed to the blue luminescence peak, and its existence is assigned to acceptor defect levels [13]. Small intense peaks observed at 482 and 492 nm are accredited to the recombination of electrons in the shallow level with the holes in the deep level [13,34]. The observed PL signatures are in accordance with spectra reported by Das *et al.* [13]. Though PL spectra showed multiple defect states, the peak profile corresponding to 468 nm was observed to be pronounced and the same was considered for biosensing measurements. For the detection of bio-analyte, ZnO nanoparticles were functionalized with the linker molecule, cysteamine. The PL spectra were recorded for ZnO-*Cys,* and the profile showed functionalization has significantly quenched the luminescence peaks of ZnO

(Fig. 3 (a-c)). AHL molecules of the uropathogen, *Pseudomonas aeruginosa* – C4 HSL and 3-oxo-C12 HSL, along with the common C6 HSL, were tested for various concentrations (Fig. 3(a-c)).

The peak intensity at 468 nm was found to increase as a function of increasing concentrations of AHL. This could be due to the possible interaction between the carbonyl group of AHLs and the amine group of cysteamine molecules (Fig. 3(e)). Thus, the defect centers are exposed, leading to the enhanced PL emission intensity in the presence of AHL molecules.

In the case of C4 HSL, the intensity of the peaks was increased significantly than ZnO and ZnO-*Cys* system. On the contrary, C6 and 3 – oxo – C12 HSLs exhibited a decreased PL intensity as compared to the ZnO. However, this intensity was higher than that of the ZnO-*Cys* system. The structural difference between C4, C6 and 3 – oxo – C12 HSLs is the carbon chain length and thereby hydrophobicity. Thus, PL intensity is inversely proportional to the hydrophobicity of the bio-analyte (AHLs). As the hydrophobicity of AHL increases, the interaction between the cysteamine and AHL decreases in-turn decreased PL intensity. The concentration-dependent sensing characteristics were investigated by varying the concentration of C4, C6, and 3-oxo-C12 HSL from 10 – 40 nM in steps of 10 nM (Fig. 3 (d)). The sensitivity of the biosensor was increased linearly with AHL concentration. To further substantiate this linear relationship, the observed trends were linearly fitted to the equations as given in Eqs. (2-4),

C4 – HSL: $y = 0.462x + 65.67, R^2 = 0.9$ (2)

C6 – HSL: $y = 0.282x + 65.67, R^2 = 0.97$ (3)

3-oxo-C_{12} HSL: $y = 1.53x - 7.33, R^2 = 0.9$ (4)

View Article Online
DOI: 10.1039/C9TB02243K

Since the R^2 values of the linearly fitted trends were approached to 0.97, it confirmed the precise linear relationship between the concentration and the sensitivity.

FTIR spectra of cysteamine, ZnO and ZnO-*Cys* system are shown in Fig.3(e). In the case of cysteamine, the presence of S-H thiol and NH_2 amines functional groups were confirmed from the peaks at 2499 and 1600 cm^{-1} respectively[35]. Zn-O functional group was identified from the characteristic peak observed at 519 cm^{-1} for both ZnO and ZnO-*Cys* system[26,27]. In the case of the ZnO-*Cys* system, the absence of the S-H thiol group confirmed the complete functionalization of cysteamine with the ZnO nanoparticles through thiol linkages[26,27]. This also indicated the absence of free cysteamine ligands in the dispersion,[26,27] which supported the optimal ratio of ZnO-Cys as 1:1. Also, the ZnO-*Cys* system has substantial amine functional groups. Usually, these amine functional groups have a strong reactivity with carbonyl groups, as reported[17]. In the present case, the carbonyl groups of AHL interacts with amine functional groups of cysteamine. This possible interaction exposes the oxygen defect centers of the ZnO nanoparticle, resulting in the enhanced PL intensity with reference to AHL concentration.

3.2.3 PL based AHL detection using ZnO-*Cys* in AUM

AUM was prepared according to the well-established protocol by Brooks and Kevil[21]. They have optimized the pH of the prepared AUM to be 6.5 (stable), among other pH values. Also, the instability of AUM was observed for higher pH values owing to the increased alkalinity at 37ºC. In addition to these reports, we have also varied the pH of AUM and investigated its influence on AHL sensitivity (Table 1). Since the maximum sensitivity of AHL in AUM was noted at 120 nM concentration (Fig. 4 (d)), the same was fixed for all pH values.

It is justified that the ZnO-*Cys* system stabilized at the pH of 6.5 showed maximum sensitivity towards C4, C6 and 3-Oxo-C12 HSLs. When the pH becomes neutral, the sensitivity was decreased marginally for all the AHLs and the same trend continued when the pH was increased 8. This might be due to the precipitation of salts present in media components[21].

The specificity of the ZnO-*Cys* in detecting AHL was validated using AUM. Fig. 4(a-c) shows the PL signatures of ZnO-*Cys* in AUM stabilized at 6.5. This media contains the necessary components to mimic natural urine. In the presence of interferences (media components), the signature peak of 468 nm was observed. The PL intensity variations for the AHLs were observed to be in the following order: C4 > C6 > 3 – oxo – C12. The peak intensity was significantly increased with AHLs concentration in the AUM without compromising the signature peak of 468 nm, which indicated that the biosensor was more stable and specific even in the presence of interfering salts in AUM. To study the concentration-dependent sensing characteristics of the biosensor in AUM, a wide range of AHLs concentrations from 10 nM to 1 µM was considered. The sensitivity of the biosensor was linearly increased with AHL concentration up-to 120 nM and saturated beyond that concentration due to the deficit cysteamine active sites for further interaction with AHLs. The obtained trends were fitted linearly with the R^2 values of 0.95 (Fig. 4(d)), confirming the linearity of the sensor.

3.2.4 Validation studies in the presence of *Pseudomonas aeruginosa*

To further validate the performance of the ZnO-*Cys* system, *Pseudomonas aeruginosa* (MCC3101) was inoculated in AUM, and the real-time response was recorded for every 30 mins (Fig. 4(e)). As mentioned earlier, *Pseudomonas aeruginosa* can produce two

View Article Online
DOI: 10.1039/C9TB02243K

AHLs: C4 HSL and 3-oxo-C12 HSL. As bacterial growth occurs, the number of AHL molecules in the diffusing media increases. Once the threshold is attained, the bacteria sense the externally accumulated AHL molecules and upregulate the group behavior. The ZnO-*Cys* system was able to detect the presence of AHL molecules from the initial time point of 30 min and reached the maximum intensity at 90 min.

A time-dependent linear response was expected, but there was a decrease in the peak intensity after 90 min. This might be due to the utilization of AHL molecules for the activation of quorum sensing in the present culture conditions. This led to the reduced concentration of the AHL molecules to be detected by the ZnO-*Cys* system. Thus, the randomness in the response is due to the dynamic nature of the biological system.

4. Conclusion

The present work deals with the development of PL based biosensor for the detection of the quorum-sensing molecule (AHL) using ZnO nanoparticles. The proof of concept was established by taking urinary tract infections as a model system. The sensitivity and specificity of the ZnO- *Cys* system were evaluated by the external addition of AHL in AUM and also in the presence of AHL producing microorganism, *Pseudomonas aeruginosa.* The PL signature peak of 468 nm was observed even in the presence of the possible interferences in AUM. The sensitivity was further confirmed in the presence of an AHL producer, *Pseudomonas aeruginosa,* in a time-dependent manner. The detection of AHL was recorded at the lag phase (30 mins) itself. Further, more studies are in line to validate the ZnO-*Cys* system in the presence of polymicrobes and the

actual urine samples. This work will pave the way to develop a point of care diagnostics to detect the infectious environment in a fast and non-invasive manner.

Conflicts of interest

There are no conflicts to declare.

Acknowledgments

Authors wish to express their sincere thanks to the Department of Science & Technology, New Delhi, India for their financial support (SR/FST/ET-II/2018/221 and ECR/2016/001805). Ms. Sahana Vasudevan and Mr. Parthasarathy Srinivasan wish to expresses their sincere thanks to DST-INSPIRE (IF170369) and Council of Scientific and Industrial Research (HRDG- 09/1095/0016/2016-EMR-I) respectively for the financial support. Authors also acknowledge SASTRA Deemed University, Thanjavur for extending infrastructure support to carry out this work. Authors would also like to thank Ms. Aishwarya Natarajan, M.Sc. SASTRA Deemed University for her technical assistance.

Notes and references

1 R. Mittal, S. Aggarwal, S. Sharma, S. Chhibber and K. Harjai, *J. Infect. Public Health*, 2009, **2**, 101–111.

2 M. R. Asadi Karam, M. Habibi and S. Bouzari, *Mol. Immunol.*, 2019, **108**, 56–67.

3 G. Córdoba, A. Holm, T. M. Sørensen, V. Siersma, H. Sandholdt, M. Makela, N. Frimodt-Møller and L. Bjerrum, *BMC Fam. Pract.*, 2018, **19**, 1–7.

4 M. Davenport, K. E. Mach, L. M. D. Shortliffe, N. Banaei, T.-H. Wang and J. C. Liao, *Nat. Rev. Urol.*, 2017, **14**, 296.

5 R. Taghadosi, M. R. Shakibaie and S. Masoumi, *Reports Biochem. Mol. Biol.*, 2015, **3**,

View Article Online
DOI: 10.1039/C9TB02243K

56–61.

6 S. Dela Ahator and L. Zhang, *Annu. Rev. Microbiol.*, 2019, **73**, 1–20.

7 Y. Yao, M. A. Martinez-Yamout, T. J. Dickerson, A. P. Brogan, P. E. Wright and H. J. Dyson, *J. Mol. Biol.*, 2006, **355**, 262–273.

8 S. Subramoni and V. Venturi, *Microbiology*, 2009, **155**, 1377–1385.

9 R. Kumar, S. Chhibber, V. Gupta and K. Harjai, *Indian J. Med. Res.*, 2011, **134**, 208–213.

10 R. Viter, A. Tereshchenko, V. Smyntyna, J. Ogorodniichuk, N. Starodub, R. Yakimova, V. Khranovskyy and A. Ramanavicius, *Sensors Actuators, B Chem.*, 2017, **252**, 95–102.

11 X. Liu, D. Huang, C. Lai, G. Zeng, L. Qin, H. Wang, H. Yi, B. Li, S. Liu, M. Zhang, R. Deng, Y. Fu, L. Li, W. Xue and S. Chen, *Chem. Soc. Rev.*, 2019, **48**, 5266–5302.

12 X. Liu, D. Huang, C. Lai, L. Qin, G. Zeng, P. Xu, B. Li, H. Yi and M. Zhang, *Small*, 2019, **15**, 1900133.

13 D. Das and P. Mondal, *RSC Adv.*, 2014, **4**, 35735.

14 H. Zeng, G. Duan, Y. Li, S. Yang, X. Xu and W. Cai, *Adv. Funct. Mater.*, 2010, **20**, 561–572.

15 A. Tereshchenko, M. Bechelany, R. Viter, V. Khranovskyy, V. Smyntyna, N. Starodub and R. Yakimova, *Sensors Actuators, B Chem.*, 2016, **229**, 664–677.

16 X. M. Wan, F. Zheng, L. Zhang, Y. Y. Miao, N. Man and L. P. Wen, *Int. J. Cancer*, 2011, **129**, 1087–1095.

17 M. Tavakkoli Yaraki, M. Tayebi, M. Ahmadieh, M. Tahriri, D. Vashaee and L. Tayebi, *J. Alloys Compd.*, 2017, **690**, 749–758.

18 M. Tayebi, M. Tavakkoli Yaraki, M. Ahmadieh, M. Tahriri, D. Vashaee and L. Tayebi, *Colloid Polym. Sci.*, 2016, **294**, 1453–1462.

19 J. M. Oliva, J. M. Ríos De La Rosa, M. J. Sayagués, J. A. Sánchez-Alcázar, P. J. Merkling and A. P. Zaderenko, *Adv. Nat. Sci. Nanosci. Nanotechnol.*,2017, **9** (1), 15001**.**

20 Dharmatti R, Phadke C, Mewada A, Pandey S, Oza G,Sharon C, Sharon M *J. Nanomedicine Res*., 2014, **1** (1), 00002.

21 T. Brooks and C. W. Keevil, *Lett. Appl. Microbiol.*, 1997, **24**, 203–206.

22 C. Y.-H. W. Z.-G. Fan Hai-Bo, Yang Shao-Yan, Zhan Pan-Feng, Wei Hong-Yuan, Liu Xian-Lin, Jiao Chun-Mei, Zhu Qin-Sheng, *Chin. Phys. Lett*, 2007, **24**, 2018.

23 S. S. Patil, M. G. Mali, M. S. Tamboli, D. R. Patil, M. V. Kulkarni, H. Yoon, H. Kim, S. S.

Al-Deyab, S. S. Yoon, S. S. Kolekar and B. B. Kale, *Catal. Today*, 2016, **260**, 126–134.

24 P. Srinivasan and J. B. B. Rayappan, *Sensors Actuators B Chem.*, 2018, **277**, 129–143.

25 P. Shankar and J. B. B. Rayappan, *RSC Adv.*, 2015, **5**, 85363–85372.

26 N. Nasrollahi, S. Aber, V. Vatanpour and N. M. Mahmoodi, *Compos. Part B Eng.*, 2018, **154**, 388–409.

27 A. Sandmann, A. Kompch, V. Mackert, C. H. Liebscher and M. Winterer, *Langmuir*, 2015, **31**, 5701–5711.

28 M. Koyano, P. QuocBao, L. thi ThanhBinh, L. HongHa, N. NgocLong and S. Katayama, *Phys. status solidi*, 2002, **193**, 125–131.

29 X. D. Gao, X. M. Li and W. D. Yu, *Mater. Sci. Eng. B*, 2004, **113**, 274–278.

30 S. Kim, H. Park, G. Nam, H. Yoon, J. S. Kim, J. S. Kim, J. S. Son, S. H. Lee and J. Y. Leem, *Bull. Korean Chem. Soc.*, 2013, **34**, 3335–3339.

31 J. Kennedy, D. A. Carder, A. Markwitz and R. J. Reeves, *J. Appl. Phys.*, 2010, **107**, 103518.

32 S. Ben Yahia, L. Znaidi, A. Kanaev and J. P. Petitet, *Spectrochim. Acta Part A Mol. Biomol. Spectrosc.*, 2008, **71**, 1234–1238.

33 B. Cao, W. Cai and H. Zeng, *Appl. Phys. Lett.*, 2006, **88**, 1–4.

34 S. Parthasarathy, V. Nandhini and B. G. Jeyaprakash, *J. Colloid Interface Sci.*, 2016, **482**, 81–88.

35 D. Dadadzhanov, (masters thesis) 2016 <https://aaltodoc.aalto.fi/handle/123456789/21642>.

View Article Online
DOI: 10.1039/C9TB02243K

Fig. 1

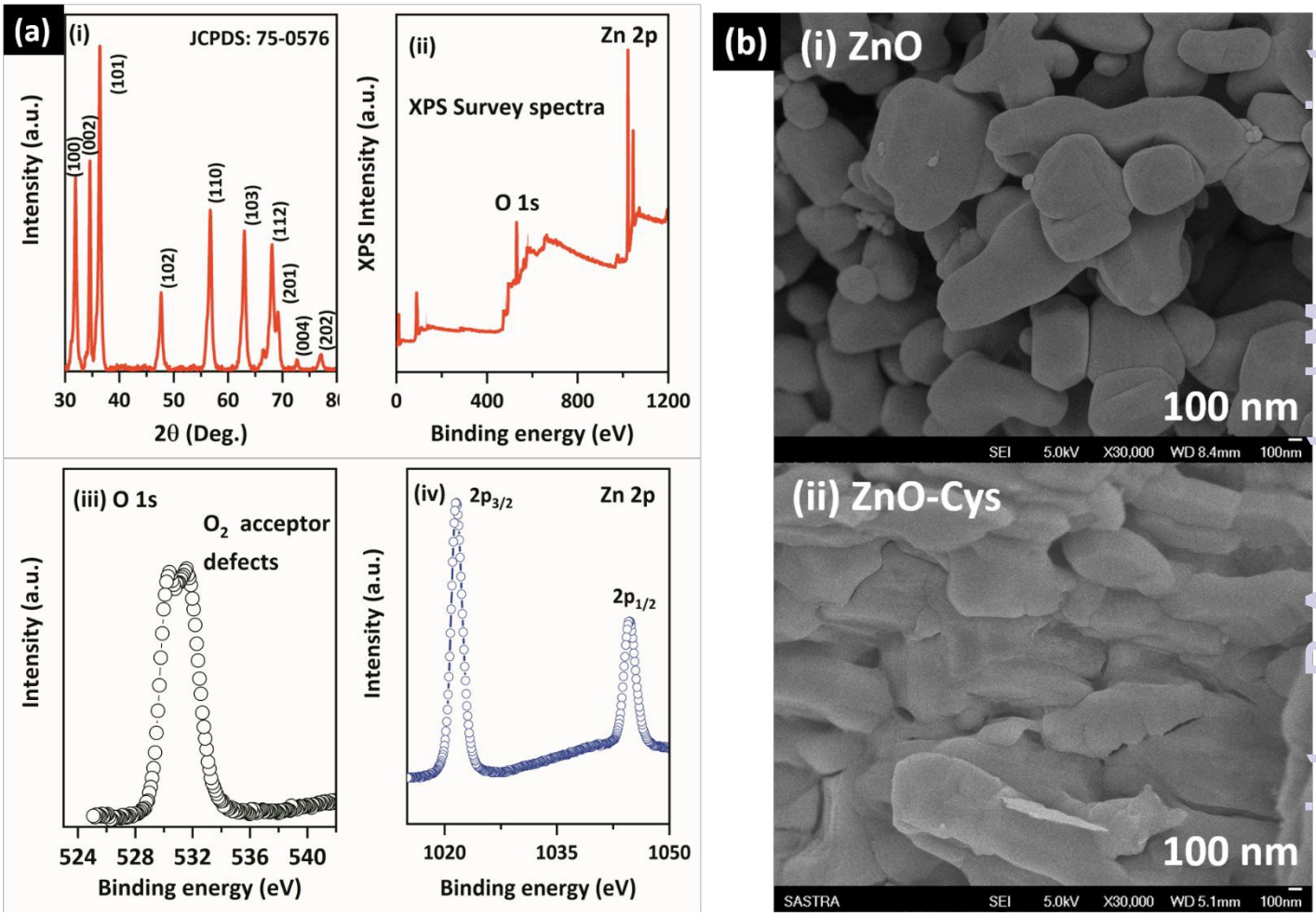

Fig. 1. (a) (i-iv) XRD pattern, XPS survey, O 1s, and Zn 2p spectra of ZnO nanoparticles, and (b) FE-SEM images of (i-ii) ZnO and ZnO-Cys nanoparticles.

View Article Online
DOI: 10.1039/C9TB02243K

Fig. 2.

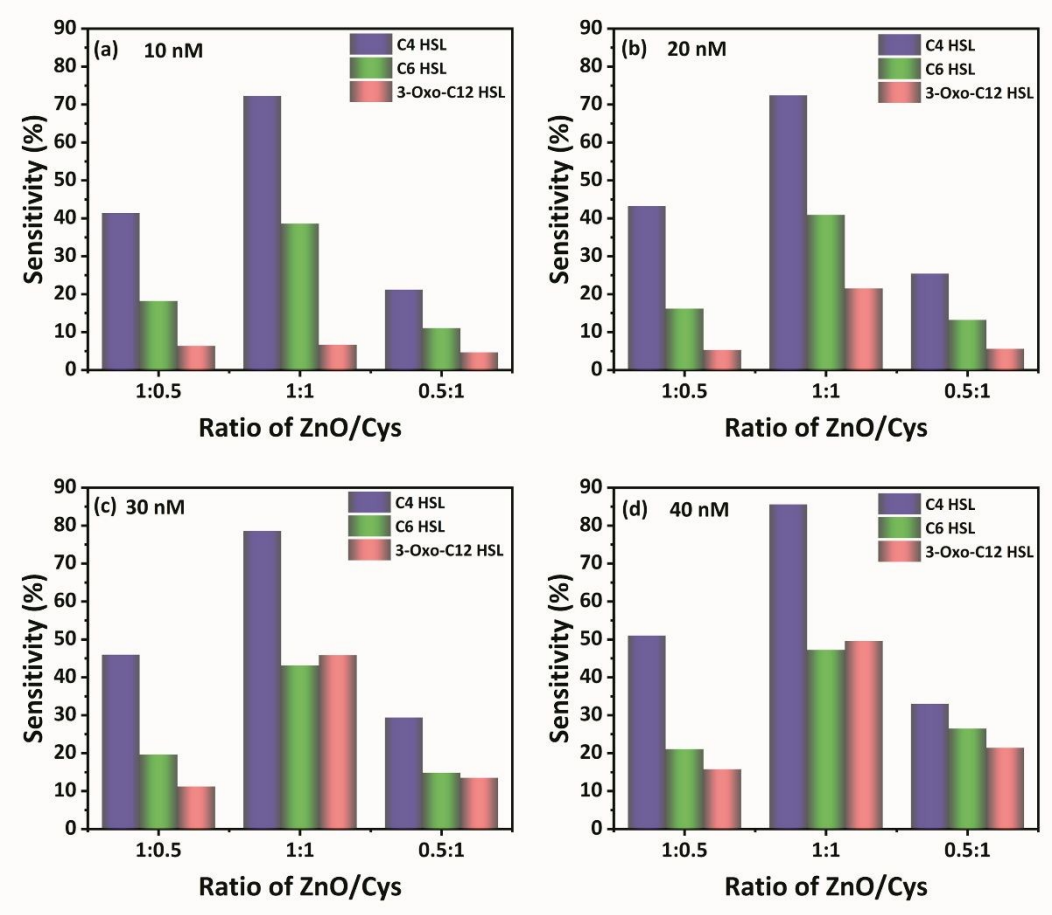

Fig. 2. Sensitivity of ZnO-Cys system at three different molar ratios of 1:0.5, 1:1, and 0.5:1 towards various concentrations of corresponding HSL (a) 10 nM, (b) 20 nM, (c) 30 nM, and (d) 40 nM.

View Article Online
DOI: 10.1039/C9TB02243K

Fig. 3.

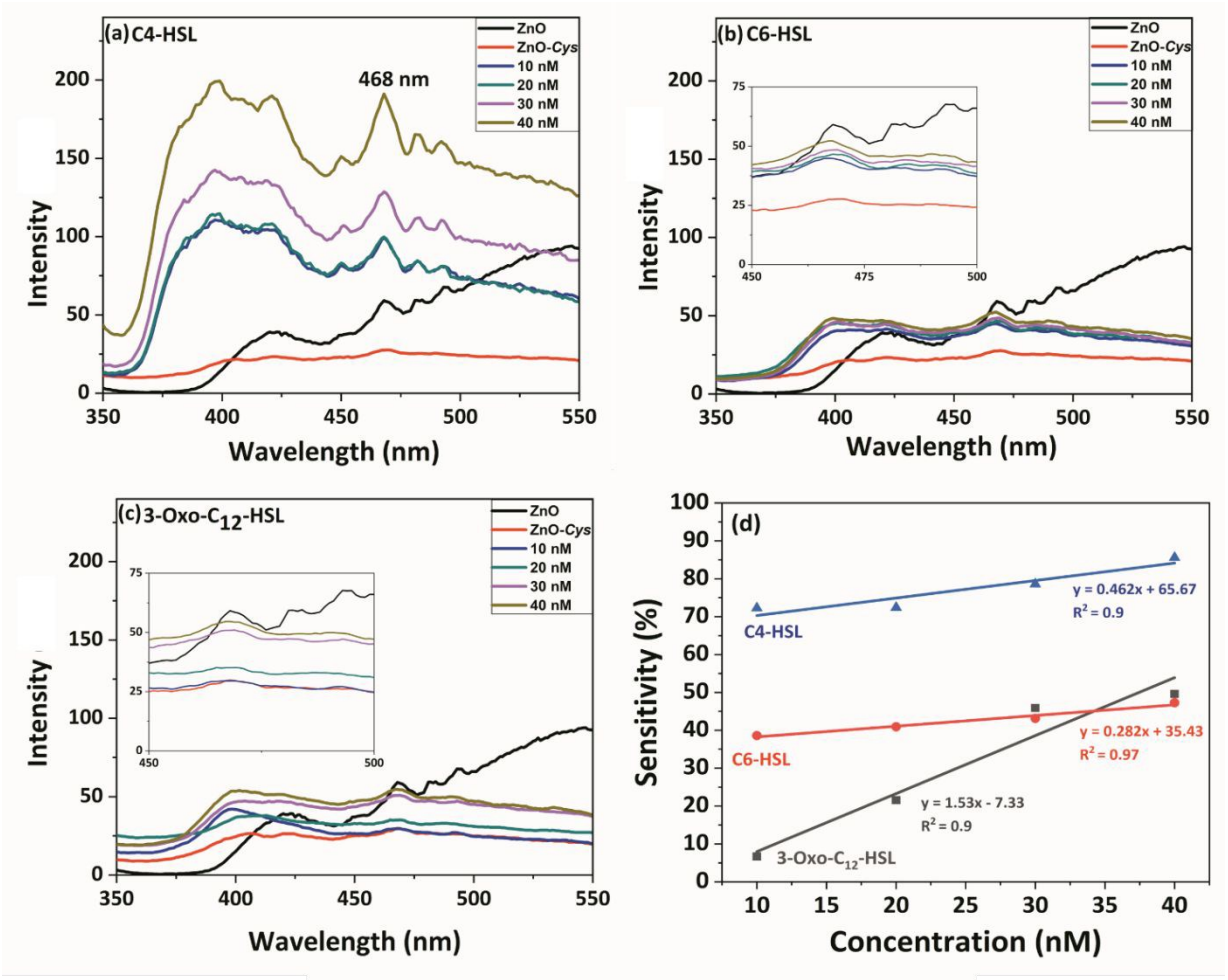

View Article Online
DOI: 10.1039/C9TB02243K

Fig 3. PL signatures of ZnO, ZnO-Cys system and corresponding AHL (a) C4-HSL, (b) C6-HSL, and (c) 3-Oxo-C12 HSL, (d) linear fitting of sensitivity and concentration of AHLs, and (e) FTIR spectra of ZnO, Cysteamine and ZnO-Cys system. (inset of (b) and (c) is the enlarged version of the peak at 468 nm.

View Article Online
DOI: 10.1039/C9TB02243K

Fig. 4.

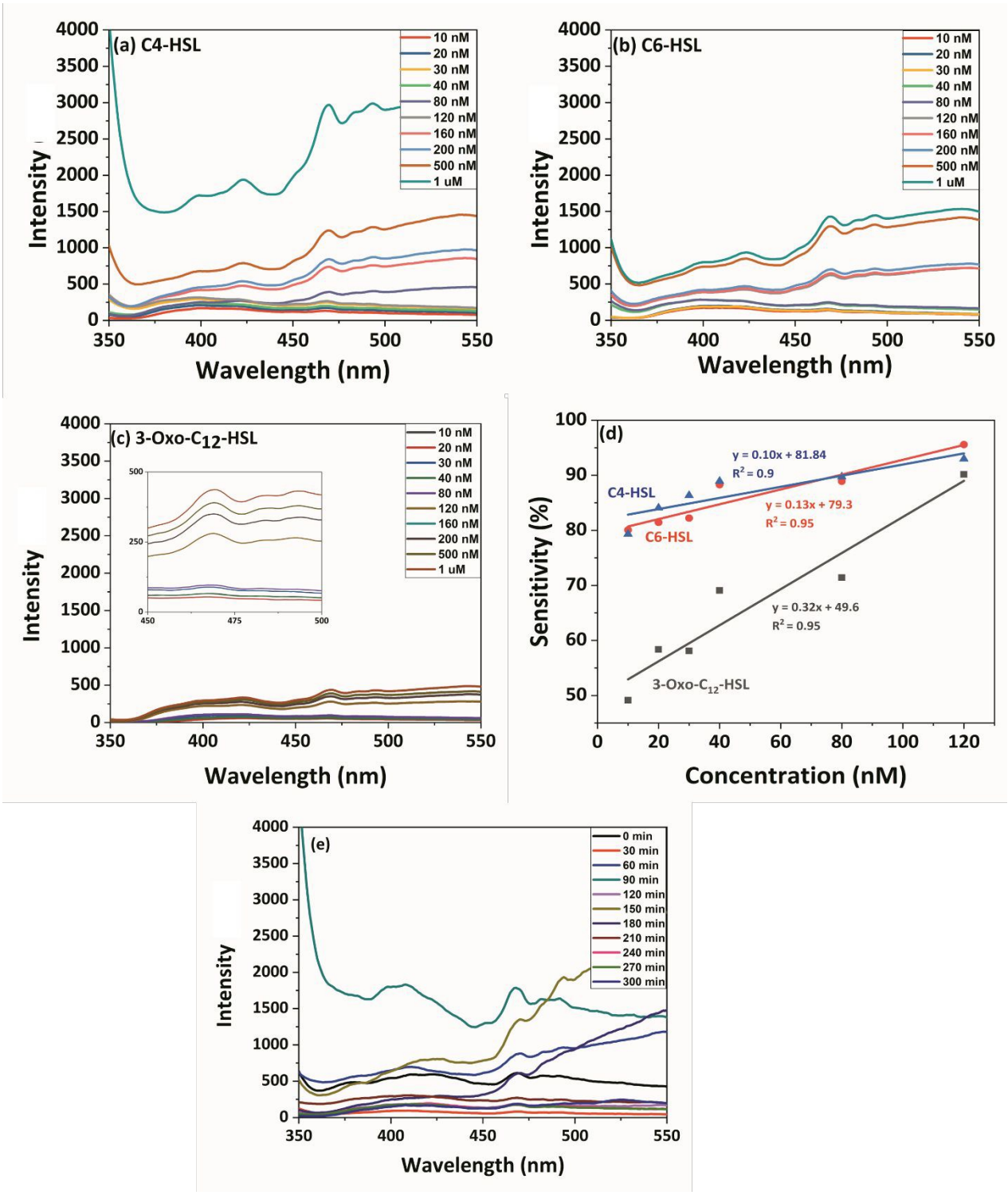

Fig 4. PL signatures of ZnO, ZnO-*Cys* system and corresponding AHL in AUM (a) C4-HSL, (b) C6-HSL, and (c) 3-Oxo-C12 HSL, and (d) linear fitting of sensitivity and concentration of AHLs, and (e) PL signatures of ZnO-*Cys* system inoculated with *Pseudomonas aeruginosa* (MCC3101).

Table 1. Bio-sensing signatures of the ZnO-*Cys* system towards 120 nM concentration of C4, C6 and 3-Oxo-C12 HSL at three different pH levels of AUM.

	C4 HSL			C6 HSL			3-Oxo-C12 HSL		
pH	**S_A**	**S_B**	**$((S_A-S_B)/S_A)$ X 100%**	**S_A**	**S_B**	**$((S_A-S_B)/S_A)$ X 100%**	**S_A**	**S_B**	**$((S_A-S_B)/S_A)$ X 100%**
6.5	392.3	27.52	92.98	623.3	27.52	95.58	279.8	27.52	90.16
7	271.22	27.35	89.91	139.79	27.35	80.43	54.31	27.35	63.19
8	123.66	26.41	78.64	142.53	26.41	81.47	66.27	26.41	60.14